Inorganica Chimica Acta 556 (2023) 121663

Contents lists available at ScienceDirect

Inorganica Chimica Acta

journal homepage: www.elsevier.com/locate/ica

Research paper

Synthesis of diaryl dithiocarbamate complexes of zinc and their uses as single source precursors for nanoscale ZnS

Jagodish C. Sarker [a,b], Firoz Alam [c], Paul McNaughter [c], David Pugh [a], Jeremy K. Cockcroft [d], David J. Lewis [c], Graeme Hogarth [a,*]

[a] Department of Chemistry, King's College London, Britannia House, 7 Trinity Street, London SE1 1DB, UK
[b] Department of Chemistry, Jagannath University, Dhaka 1100, Bangladesh
[c] Department of Materials, University of Manchester, Oxford Road, Manchester M13 9PL, UK
[d] Department of Chemistry, University College London, 20 Gordon Street, London WC1H 4AJ, UK

ARTICLE INFO

Keywords:
Diaryl dithiocarbamate
Zinc complexes
Single source precursors
Amine-exchange

ABSTRACT

Diaryldithiocarbamate complexes, $[Zn(S_2CNAr_2)_2]$, have been prepared with a view to comparing their structures, reactivity and thermally-promoted degradation with respect to the well-studied dialkyl-derivatives. In the solid-state both $[Zn\{S_2CN(p\text{-}tol)_2\}_2]$ and $[Zn\{S_2CN(p\text{-}anisyl)_2\}_2]$ are monomeric with a distorted tetrahedral Zn (II) centre, but somewhat unexpectedly, the bulkier naphthyl-derivative $[Zn\{S_2CN(2\text{-}nap)_2\}_2]_2$ forms dimeric pairs with five-coordinate Zn(II) centres. Preliminary reactivity studies on $[Zn\{S_2CN(p\text{-}tol)_2\}_2]$ suggests that it binds amines and cyclic amines in a similar fashion to the dialkyl complexes and can achieve six-coordination as shown in the molecular structure of $[Zn\{S_2CN(p\text{-}tol)_2\}_2(2,2'\text{-bipy})]$. The thermal decomposition of $[Zn\{S_2CN(p\text{-}tol)_2\}_2]$ was studied in oleylamine solution by both heat-up and hot-injection methods. Nanorods of ZnS were produced in both cases with average dimensions of 17 × 2.1 nm and 11 × 3.5 nm respectively, being significantly shorter than those produced from $[Zn(S_2CN^iBu_2)_2]$ under similar conditions. This is tentatively attributed to the differing rates of amine-exchange between diaryl- and dialkyl dithiocarbamate (DTC) complexes and/or their differing rates of DTC loss following amine-exchange. The solid-state decomposition of $[Zn\{S_2CN(p\text{-}tol)_2\}_2]$ has also been studied at 450 °C under argon affording irregular and large (10–300 μm) sheet-like particles of wurtzite.

1. Introduction

ZnS is an intrinsic *n*-type semiconductor that finds use in optoelectronic devices due to its unique photoluminescence and electroluminescence properties [1]. Two crystalline forms are known, sphalerite (cubic, β) and wurtzite (hexagonal, α), with band gaps of 3.72 and 3.77 eV respectively. While there are many different strategies towards the synthesis of nanoscale ZnS, the single source precursor (SSP) approach is especially appealing as it allows control of nanoparticulate shape-size-structure without the need for elaborate experimental facilities. In this context, air and moisture stable zinc dithiocarbamate (DTC) complexes [2] have found widespread use, initially in chemical vapour deposition (CVD) studies to deposit thin films and more recently under solvothermal conditions to produce ZnS nanowires and nanorods [3]. The first solvothermal synthesis of ZnS (wurtzite) nanowires was reported in 2010 via the decomposition of $[Zn(S_2CNEt_2)_2]$ in oleylamine (OLA) at 300 °C [4]. The wires produced had an extremely high aspect ratio being ca 300 nm long but only 4 nm in diameter. More recently, we have reported that changing the nature of the DTC substituents has a significant effect upon the wires produced [5]. Thus, a similar heat-up decomposition of $[Zn(S_2CN^iBu_2)_2]$ in OLA at 230 °C gave materials best described as nanorods with dimensions of ca. 35 nm × 3 nm [5]. The physical form of the nanomaterials can also be controlled by varying the decomposition conditions. Thus, decomposition of $[Zn(S_2CNBu_2)_2]$ in a mixture of dodecylamine (DDA) and PPh_3 at 280 °C affords ultrathin nanowires with diameters of ca. 2 nm and lengths of up to 10 μm [6], while decomposition of $[Zn(S_2CNEt_2)_2]$ in aqueous hydrazine hydrate at 150–200 °C afforded nanorods with diameters of between 6 and 30 nm, varying as a function of temperature and time [7].

A long-standing goal in our research on metal-DTC complexes as SSPs to nanoscale metal sulfides has been to better understand their decomposition mechanism(s) so as to be able to control the overall

* Corresponding author.
E-mail address: graeme.hogarth@kcl.ac.uk (G. Hogarth).

https://doi.org/10.1016/j.ica.2023.121663
Received 18 May 2023; Received in revised form 21 June 2023; Accepted 23 June 2023
Available online 25 June 2023

decomposition process and consequently the size, shape, phase etc. of the generated nanomaterials [8–12]. In our earlier work on the solvothermal decomposition of $[Zn(S_2CNMe_2)_2]$ in OLA [5] we used *in situ* X-ray absorption spectroscopy (XAS) to show that OLA initially binds to the zinc centre to form $[Zn(S_2CNMe_2)_2(OLA)]$, which is stable up to ca. 70 °C. Above this temperature, OLA dissociates and at ca. 90 °C decomposition to ZnS occurs, a process which is activated by amine-exchange. The latter results in exchange of a secondary for a primary DTC ligand and in the OLA (pH ca. 14) the backbone proton is immediately removed which triggers decomposition and affords a low temperature route to ZnS (Scheme 1).

In further developing low temperature solvothermal routes to metal-sulfide nanomaterials, we targeted diaryl dithiocarbamate complexes in the belief that the electron-withdrawing nature of the aryl substituents would facilitate low temperature amine-exchange, a process which occurs via attack of the primary amine at the electrophilic backbone carbon of the secondary amine DTC ligand [8]. Our initial experiments suggest that this strategy is well-conceived and has led to low temperature solvothermal routes to CoS_2 [13] and CuS [14] from diaryl-DTC precursors $[Co(S_2CNAr_2)_3]$ and $[Cu(S_2CNAr_2)_2]$ respectively. In contrast to their dialkyl-DTC counterparts, diaryl-DTC complexes are relatively rare [2] and few have been fully characterised prior to our work. This extends to zinc derivatives, of which there are no well-characterised examples in the recent literature. Herein, we report the preparation of several $[Zn(S_2CNAr_2)_2]$ complexes, together with structural studies in order to compare them with the dialkyl-derivatives. We also show that, like the dialkyl-derivatives, they can further coordinate amines, and we develop one of these, namely $[Zn\{S_2CN(p\text{-}tol)_2\}_2]$ as a SSP to ZnS nanomaterials.

2. Experimental

2.1. General procedures

All solvents and chemicals were purchased from Sigma-Aldrich or Alfa Aesar and used without any further purification. ^{1}H NMR and ^{13}C{^{1}H} NMR spectra were recorded on a Bruker Advance III 400 MHz spectrometer using the residual protons from either DMSO-d_6 or $CDCl_3$ as a reference. IR spectroscopy was conducted using either Perkin Elmer Spectrum 2 FTIR or Shimadzu Affinity IR spectrophotometers. Mass spectra were obtained using a Micromass 70-SE spectrometer utilising electrospray ionisation (ESI). Elemental analyses were performed using a Flash 2000 Organic Elemental Analyzer at the Science Centre, London Metropolitan University. PXRD patterns were measured at University College London on a Bruker AXS D4 diffractometer using Cu Kα1 radiation. Diffraction patterns obtained were compared to database standards. TEM images were obtained using a JEOL-1010 microscope at 100 kV equipped with a Gatan digital camera. A 4 mL droplet of nanoparticle suspension ($CHCl_3$) was placed on a holey carbon-coated copper TEM grid and allowed to evaporate in air under ambient laboratory conditions for several minutes. Lithium dithiocarbamate salts **1a-g** were prepared as previously reported [13].

2.2. Synthesis of $[Zn(S_2CNAr_2)_2]$ (2a-g)

$[Zn(S_2CNPh_2)_2]$ (2a): **1a** (126 mg, 0.50 mmol) and $[Zn(CH_3CO_2)_2]$ (45.9 mg, 0.25 mmol) were dissolved in water (10 mL) and stirred for 10 min at room temperature. The white precipitate obtained was filtered, washed with water, the residual water was allowed to evaporate and the product **2a** was air dried. Similar scale reactions and procedures were followed for **2b-g**. All are air stable solids.

2a (Ar = Ph): White crystals, 138 mg, 100% yield. Elemental Analysis: Anal. Calcd. for **2a**.$^1/_3CH_2Cl_2$: C, 54.33; H, 3.58; N, 4.81 %. Found: C, 54.85; H, 3.67; N, 4.89 %. IR (solid) (cm^{-1}): 687, 746, 1004, 1034, 1053, 1385, 1488. ^{1}H NMR ($CDCl_3$): δ 7.45 (m, 8 H), 7.39 (m, 8 H), 7.32 (m, 4 H). ^{13}C{^{1}H} NMR ($CDCl_3$): δ 210.6 (C═N), 145.7, 129.5, 128.4, 126.87. ESI-MS: *m/z* 552.98 (M^+, 50%), 246.04 (M^+−4Ph, 100%).

2b (Ar = p-MeC_6H_4): White crystals, 117 mg, 77 % yield. Elemental Analysis: Anal. Calcd. for $C_{30}H_{28}N_2S_4Zn$: C, 59.05; H, 4.62; N, 4.59%. Found: C, 59.25; H, 4.73; N, 4.50 %. IR (solid) (cm^{-1}): 550, 589, 755, 810, 1038, 1504. ^{1}H NMR ($CDCl_3$): δ 7.24 (d, J = 8 Hz, 8 H), 7.10 (d, J = 8 Hz, 8 H), 2.25 (s, 12 H). ^{13}C{^{1}H} NMR ($CDCl_3$): δ 210.2 (C═N), 143.5, 138.3, 130.3, 126.4, 21.2. ESI-MS: *m/z* 608 (M^+), 872 (M^++Tol_2DTC).

2c (Ar = p-$MeOC_6H_4$): White crystals, 116 mg, 69% yield. Elemental Analysis: Anal. Calcd. for **2c**.$^1/_2CHCl_3$: C, 49.92; H, 3.91; N, 3.82 %. Found: C, 49.79; H, 4.12; N, 3.81 %. IR (solid) (cm^{-1}): 598, 817, 1034, 1242, 1297, 1501. ^{1}H NMR ($CDCl_3$): δ 7.26 (dd, 8H, J = 4, 8 Hz), 6.80 (dd, 8H, J = 4, 8 Hz), 3.72 (s, 12 H). ^{13}C{^{1}H} NMR ($CDCl_3$): δ 210.5 (C═N), 159.1, 139.5, 127.7, 114.7, 55.5. ESI-MS: *m/z* 673.03 (M^+, 60%), 230.12 (M^+−2MeOC_6H_4-N(MeOC_6H_4)$_2$, 100%).

2d (Ar = 2,2́-dinaphthyl): Off white crystals,138 mg 74% yield. Elemental Analysis: Anal. Calcd. for **2d**.$^1/_2CH_2Cl_2$: C, 64.07; H, 3.67; N, 3.52 %. Found: C, 64.85; H, 3.62; N, 3.54 %. IR (solid) (cm^{-1}): 474, 546, 745, 756, 773, 812, 1043, 1229, 1269, 114, 1331, 1369, 1506, 1597, 1628. ^{1}H NMR ($CDCl_3$): δ 7.96 (s, 3 H), 7.83 (m, 11 H), 7.66 (m, 4 H), 7.48 (m, 7 H), 7.43 (t, 1 H, J = 8 Hz), 7.33 (m, 2 H). ^{13}C{^{1}H} NMR ($CDCl_3$): δ 210.9 (C═N), 143.3, 140.8, 134.8, 133.5, 132.7, 129.7, 128.4, 127.9, 127.2, 129.9, 125.9, 124.8, 120.4, 112.4.

2e (Ar = Ph, m-$MeOC_6H_4$): White crystals, 120 mg, 78% yield. Elemental Analysis: Anal. Calcd. for $C_{28}H_{24}N_2O_2S_4Zn$: C, 55.36; H, 3.98; N, 4.61 %. Found: C, 55.79; H, 3.84; N, 4.35 %. IR (solid) (cm^{-1}): 505, 623, 656, 687, 696, 733, 772, 833, 926, 1049, 1138, 1225, 1285, 1362, 1485, 1585, 1603. ^{1}H NMR ($CDCl_3$): δ 7.42 (d, J = 8 Hz, 4 H), 7.36 (t, J = 8 Hz, 4 H), 7.26 (m, 4 H), 7.00 (d, J = 8 Hz, 2 H), 6.96 (t, J = 4 Hz, 2 H), 6.82 (d, J = 4 Hz, 2 H), 3.76 (s, 6 H).^{13}C{^{1}H} NMR ($CDCl_3$): δ 210.6 (C═N), 160.4, 146.7, 145.8, 130.3, 129.6, 129.5, 128.58, 126.9, 119.1, 118.4, 114.2, 112.85, 55.6.

2f (Ar = Ph, 1-Naphthyl): Off white crystals, 160 mg, 98% yield. Elemental Analysis: Anal. Calcd. for **2f**.$^1/_2CHCl_3$: C, 58.05; H, 3.46; N, 3.92 %. Found: C, 58.25; H, 3.48; N, 3.81 %. IR (solid) (cm^{-1}): 528, 625, 690, 725, 766, 779, 797, 889, 1005, 1024, 1057, 1086, 1267, 1307, 1341, 1354, 1389, 1489, 1593. ^{1}H NMR ($CDCl_3$): δ 7.86 (m, 8 H), 7.58 (dd, J = 4, 8 Hz, 2 H), 7.50 (m, 8 H), 7.41 (m, 4 H), 7.32 (m, 2 H). ^{13}C{H} NMR ($CDCl_3$): δ 211.8 (C═N), 145.9, 142.6, 134.7, 129.5, 129.4, 128.9, 128.8, 128.5, 127.7, 126.8, 126.4, 125.8, 125.4, 123.3.

2 g (Ar = Ph, 2-Naphthyl): Off white crystals, 128 mg, 79% yield.

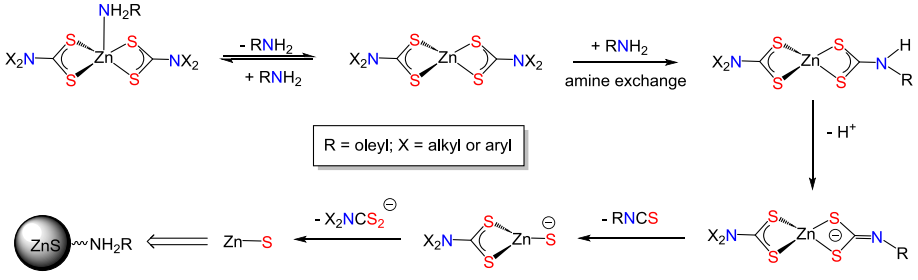

Scheme 1. Proposed decomposition mechanism of $[Zn(S_2CNX_2)2$ (X = alkyl e.g. Me) in primary amines (RNH_2).

Elemental Analysis: Anal. Calcd. for **2g**.$^1/_3CHCl_3$: C, 59.45; H, 3.54; N, 4.04 %. Found: C, 59.70; H, 3.58; N, 3.96 %. IR (solid) (cm^{-1}): 474, 559, 664, 691, 729, 745, 787, 810, 1042, 1233, 1265, 1339, 1364, 1489, 1506, 1591. ^{1}H NMR ($CDCl_3$): δ 8.22 (m, 2 H), 7.87 (m, 4 H), 7.56 (m, 12 H), 7.37 (m, 4 H), 7.28 (m, 2 H). ^{13}C{H} NMR ($CDCl_3$): δ 210.8 (C═N), 145.9, 143.2, 133.5, 132.7, 130.0, 129.8, 129.7, 129.6, 128.6, 128.4, 127.9, 127.7, 127.4, 127.2, 127.1, 126.9, 126.6, 125.8, 125.4, 124.7. ESI-MS: *m/z* 652.3 (M^+).

2.3. Synthesis of adducts of [Zn{S_2CN(p-tolyl)$_2$}$_2$] (2b)

2b (100 mg, 0.165 mmol) and 2,2′-bipyridine, (bipy) (26 mg, 0.165 mmol) were dissolved in toluene (10 mL) and stirred overnight at room temperature. A pale-yellow precipitate resulted suspended in a white/milky solution. The solvent was removed under reduced pressure and the resulting solid washed with water and hexanes. Air drying afforded [Zn{S_2CN(p-tolyl)$_2$}$_2$(bipy)] (**5**) (92 mg, 74 %). Following a similar procedure with pyridine (py) and cyclohexylamine ($CyNH_2$) afforded pale yellow solids of [Zn{S_2CN(p-tolyl)$_2$}$_2$(py)] (**3**) (73 mg, 65 %) and [Zn{S_2CN(p-tolyl)$_2$}$_2$(NH_2Cy)] (**4**) (73 mg, 63 %) respectively.

3 Yellow crystals, 73 mg, 65% yield. Elemental Analysis: Anal. Calcd. for $C_{36}H_{40}N_3S_4Zn$**:** C, 61.04; H, 5.69; N, 5.93 %. Found: C, 61.41; H, 5.88; N, 6.19 %. ^{1}H NMR ($CDCl_3$): δ 8.92 (m, 2 H), 7.87 (m, 1 H), 7.47 (m, 2 H), 7.34 (m, 8 H), 7.18 (m, 8 H), 2.32 (s, 12 H). ^{13}C{^{1}H} NMR ($CDCl_3$): δ 211.1 (CS_2), 149.6, 144.2, 138.0, 130.1, 126.8, 124.8, 118.0, 21.3. ESI-MS: *m/z* 689.31 (M^+).

4 Pale yellow crystals, 73 mg, 63% yield. Elemental Analysis: Anal. Calcd. for $C_{35}H_{33}N_3S_4Zn$**:** C, 60.99; H, 4.83; N, 6.10 %. Found: C, 61.31; H, 4.89; N, 6.25 %. ^{1}H NMR ($CDCl_3$): δ 7.14 (d, *J* = 8 Hz, 8 H), 7.00 (d, *J* = 8 Hz, 8 H), 2.50 (m, 1 H), 2.16 (s, 12 H), 1.70 (m, 2 H), 1.58 (m, 2 H), 1.47 (m, 1 H), 1.40 (s, 1 H), 1.11 (m, 2 H), 0.93 (m, 3 H). ^{13}C{^{1}H} NMR ($CDCl_3$): δ 211.8 (C═N), 144.7, 137.0, 129.6, 126.3, 117.6, 50.3, 36.6, 25.5, 25.0, 20.9.

5 Pale yellow crystals, 92 mg, 74% yield. Elemental Analysis: Anal. Calcd. for $C_{40}H_{36}N_4S_4Zn$**:** C, 62.69; H, 4.74; N, 7.31 %. Found: C, 62.96; H, 4.87; N, 7.38 %. ^{1}H NMR ($CDCl_3$): δ 9.03 (d, *J* 4 Hz, 1 H), 8.85 (d, *J* 4 Hz, 1 H), 8.17 (t, *J* 8 Hz, 2 H), 8.05 (t, *J* 4 Hz, 1 H), 7.86 (t, *J* 8 Hz, 1 H), 7.54 (t, *J* 8 Hz, 1 H), 7.40 (m, 1 H), 7.30 (d, *J* 8 Hz, 8 H), 7.13 (d, *J* 8 Hz, 8 H), 2.30 (s, 12 H). ^{13}C{^{1}H} NMR ($CDCl_3$): δ 149.4, 144.7, 140.3, 138.3, 137.6, 130.0, 126.9, 126.6, 124.9, 120.9, 120.8, 21.3. ESI-MS: *m/z* 766.49 (M^+).

2.4. Single crystal X-ray diffraction

We thank the EPSRC UK National Crystallography Service at the University of Southampton for the collection of the crystallographic data for **2d** and **5** [15]. A Rigaku FRE+ diffractometer (Mo-K_α radiation, 0.71073 Å) was used equipped with HF Varimax confocal mirrors, an AFC12 goniometer, HG Saturn 724+ detector, and an Oxford Cryosystems low-temperature device. Datasets were processed using CrysAlisPro [16] and solutions were solved and refined using Olex-2 [17]. Data for **2b** and **2c** were collected at University College London using a SuperNova, Dual, Cu at zero, Atlas diffractometer. Structures were solved using Olex2 [17] and the Olex2.solve [18] structure solution program with Charge Flipping and were refined with SHELXL [19] using least squares minimization. CCDC reference numbers 2263849 (**2b**), 2263850 (**2c**), 2263851 (**2d**) and 2263852 (**5**) contain crystallographic data in CIF format which is summarised in Table S1.

2.5. Solvothermal heat-up (HU) process

2b (25 mM) was added to OLA (20 mL) in a three-neck round bottom flask attached to a condenser which was evacuated and refilled with N_2 repeatedly for 15 min. The solution was then heated to 230 °C and held at this temperature for 1 h. The mixture was slowly cooled to room temperature, whereupon MeOH (80 mL) was added with stirring. The mixture was centrifuged, and the solution decanted to give the resultant nanoparticles. These were redispersed in MeOH (80 mL), a procedure that was carried out three times, and finally in CH_2Cl_2 (80 mL). Following this, the material was air-dried.

2.6. Solvothermal hot-injection (HI) process

OLA (15 mL) was added into a 3-necked round bottom flask attached to a condenser which was evacuated and refilled with N_2 repeatedly on a Schlenk line for ca. 15 min. When the temperature was at 230 °C, 300 mg of **2b** (dissolved in 5 mL OLA, heated for 15 min in oven at ca. 80 °C) was injected into the 3-necked round bottom flask. The colour immediately changed from dark brown to dark black. The solution was heated to 230 °C and held there for 1 h. The mixture was slowly cooled to room temperature, whereupon MeOH (80 mL) was added with stirring. The mixture was centrifuged, and the solution decanted to give the resultant nanoparticles. These were washed three times with 80 mL MeOH and once with 80 mL CH_2Cl_2 (as detailed above) and then air-dried.

2.7. Dry decomposition

Thermolysis was carried out by heating **2b** (placed in a ceramic boat and positioned in the centre of a Carbolite MTF furnace) to 450 °C and kept at this temperature for one hour under argon to produce ZnS. The final powders were collected after cooling to room temperature.

3. Results and discussion

3.1. Synthesis and molecular structures of [Zn(S_2CNAr$_2$)$_2$]

As discussed in a previous paper, the lithium salts LiS_2CNAr_2 (**1a-g**) are conveniently using BuLi as a base and are air and moisture stable, thus making them excellent diaryl-dithiocarbamate sources [13]. Addition of ca. two equivalents of **1a-g** to zinc acetate in water resulted in the immediate formation of off-white precipitates and after filtration and washing afforded [Zn(S_2CNAr$_2$)$_2$] (**2a-g**) in high yields (ca. 90 %) (Scheme 2). ^{1}H NMR spectra confirmed the DTC inclusion as did ^{13}C{^{1}H} NMR spectra which showed a characteristic signal at ca. 212–210 assigned to the backbone carbon. ESI-MS spectra show molecular ion peaks and other characterising data are in full agreement with the molecular formula.

Numerous structural studies have been carried out on zinc dialkyl DTC complexes [2,20–34] with three distinct motifs being found (Fig. 1). Most common are centrosymmetric dimers with one terminal and one bridging DTC ligand per zinc centre of which there are two structural types, boat-saddle or a twisted-chair conformations, differing with respect to the relative orientations of the two bridging DTCs. The secondary Zn-S interactions within both types are of the order of 2.8–3.0 Å, whereas the primary Zn-S interactions are of 2.3–2.5 Å [2]. The dimeric forms also have relatively short Zn…Zn distances of ca. 3.5–4.0 Å. The tetrahedral mononuclear form is adopted in complexes with large alkyl substituents, which make dimer formation unfavourable [2,20].

Since zinc diaryl-DTC complexes have not been previously characterized by X-ray crystallographically, we analysed single crystals of **2b** and **2c** (Fig. 2) which were obtained upon layering $CHCl_3$ solutions of **2b-c** with hexanes. While the quality of the data for **2b** is poor due to twinning, we include the structure here as the gross structural features are accurate. Both are monomeric with distorted tetrahedral zinc centres, demonstrated by tau-4 parameters of 0.72 and 0.68 respectively, and the S-Zn-S angles and Zn-S distances do not vary significantly from the corresponding dialkyl derivatives [2,20].

We have also crystallographically characterised the di(2-naphthyl) derivative **2d** which we expected would be monomeric. However, it adopts a twisted chair centrosymmetric dimeric structure (Fig. 3) similar to those observed for [Zn(S_2CNEt$_2$)$_2$] [21], [Zn(S_2CNPr$^i_2$)$_2$] [23] [Zn(S_2CNMeR)$_2$] (R = Et, Pr, Pr^i, Bu) [25] and [Zn(S_2CNEtPh)$_2$] [34]. The

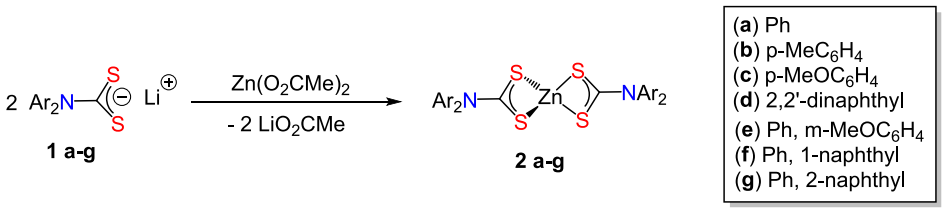

Scheme 2. Synthesis of $[Zn(S_2CNAr_2)_2]$ (**2a-g**).

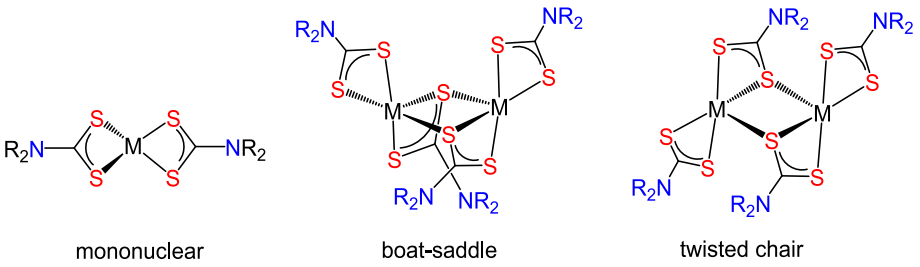

Fig. 1. Solid-state structural types for $[Zn(S_2CNR_2)_2]_n$.

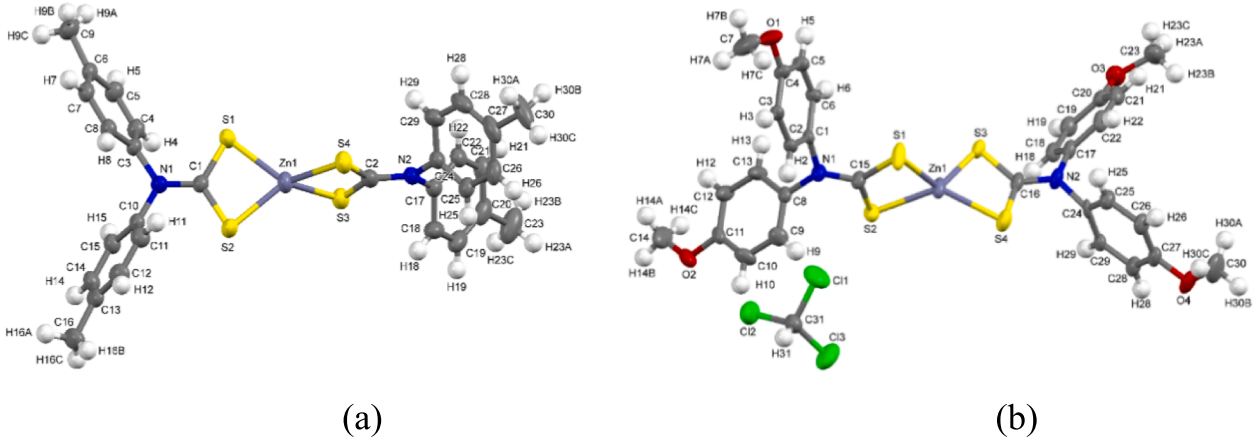

Fig. 2. Molecular structures of (a) $[Zn\{S_2CN(p\text{-}tol)_2\}_2]$ (**2b**) and (b) $[Zn\{S_2CN(p\text{-}anisyl)_2\}_2].CHCl_3$ (**2c**).

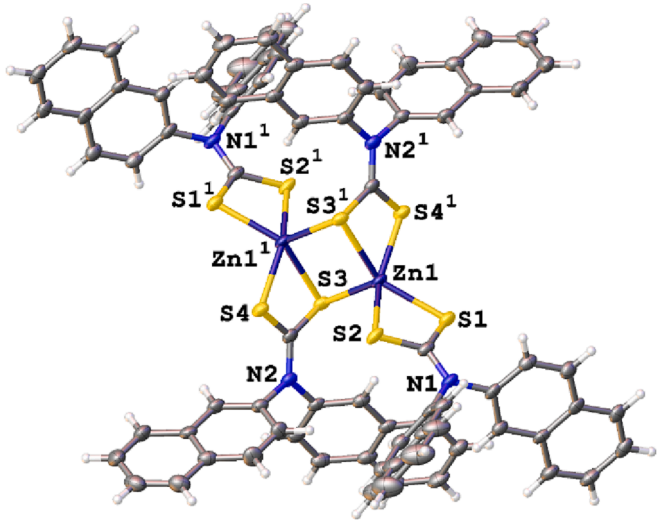

Fig. 3. Molecular structure of $[Zn\{S_2CN(2\text{-}nap)_2\}_2]_2$ (**2d**).

chelate ligands at a single centre tend to have three short [2.3–2.5 Å] and one long [2.7–2.9 Å] Zn-S bonds, while the intermolecular Zn-S interaction is also short [2.3–2.4 Å] [20]. In **2d** all Zn-S bonds are of similar lengths ranging only between 2.389 and 2.511 Å and the tau-5 parameter of 0.24 suggests that the overall structure at zinc is best described as a heavily distorted square-based pyramid.

3.2. Synthesis of N-donor adducts of $[Zn\{S_2CN(p\text{-}tol)_2\}_2]$ and the molecular structure of $[Zn\{S_2CN(p\text{-}tol)_2\}_2(2,2'\text{-}bipy)]$

As first reported in the late 1960s, a wide variety of five-coordinate $[Zn(S_2CNR_2)_2(L)]$ have been prepared with nitrogen-containing bases adopting a geometry intermediate between a square pyramid and trigonal bipyramid in the solid state [2], while six-coordinate adducts $[Zn(S_2CNR_2)_2(L_2)]$ are formed upon addition of 2,2′-bipyridine (2,2′-bipy) and 1,10-phenanthroline (1,10-phen) [2]. To establish if similar adducts could be formed with diaryl-DTC complexes, room temperature reactions of **2b** with pyridine, cyclohexylamine and 2,2′-bipy were carried out resulting in formation of pale-yellow adducts $[Zn\{S_2CN(p\text{-}tol)_2\}_2(py)]$ (**3**) and $[Zn\{S_2CN(p\text{-}tol)_2\}_2(NH_2Cy)]$ (**4**) and $[Zn\{S_2CN(p\text{-}tol)_2\}_2(2,2'\text{-}bipy)]$ (**5**) respectively in moderate yields (63–74%). All were characterised by spectroscopic data being similar to related adducts [35–37] and elemental analyses are consistent with their

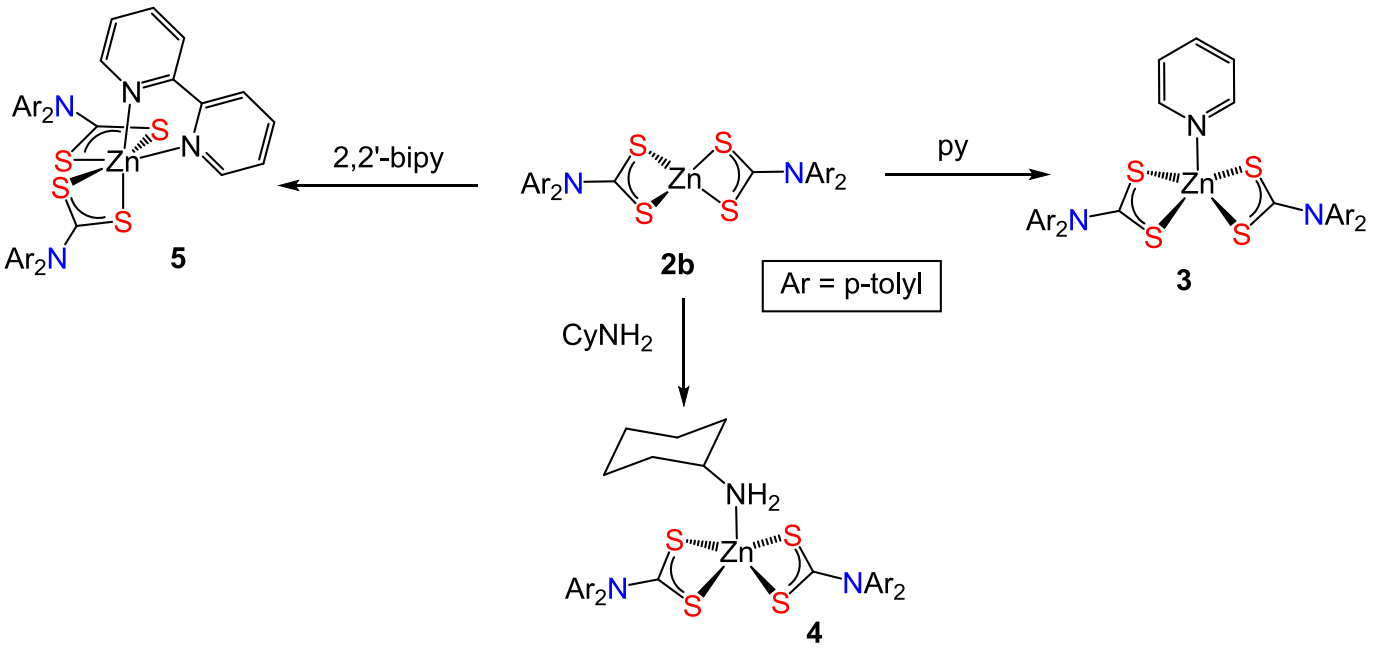

Scheme 3. Synthesis of *N*-donor adducts of **2b**.

formulation (See Scheme 3).

Several 2,2′-bipy adducts of dialkyl-DTC complexes have been reported [38] with some being crystallographically characterised [39–41]. For comparison, an X-ray structural study was carried out on **5**.$CHCl_3$, suitable crystals resulting upon layering $CHCl_3$ solutions with hexanes at room temperature. Data are given in Table S1. The overall structure is complex as there are eight molecules of solvent and four independent molecules of **5** in the unit cell, one of which is shown in Fig. 4. The zinc centre adopts a distorted octahedral geometry with two distinct Zn-S bonds [Zn1-S1 2.4615(3), Zn1-S2 2.5886(3) Å], the shorter of which lies *trans* to nitrogen [N2-Zn1-S1 155.21°].

3.3. *[Zn{S_2CN(p-tol)$_2$}$_2$] (**2b**) as a single source precursor (SSP) to ZnS*

We selected the bis(p-tolyl) derivative [Zn{S_2CN(p-tol)$_2$}$_2$] (**2b**) for the thermal decomposition studies as it shows better solubility than the diphenyl-DTC complex **2a** in a range of organic solvents and in primary amines. We initially looked at the TGA of **2b** in order to compare its dry decomposition with that of the well-studied [Zn(S_2CNEt$_2$)$_2$] [42] for which decomposition begins around ca. 220 °C and is complete at 340 °C. As shown (Fig. 5) decomposition of **2b** occurs over a similar but narrower range, starting at ca. 275 °C and being complete by ca. 320 °C. The residual mass of ca. 21% is slightly higher than would be expected for formation of ZnS. Based on this, dry thermolysis of a powdered sample of **2b** was carried out at 450 °C to ensure complete conversion to ZnS. The furnace was kept at this temperature for 1 h under argon and gave a grey powder which was collected after cooling.

Dissolution of [Zn{S_2CN(p-tol)$_2$}$_2$] (**2b**) in warm OLA gave a yellow solution, likely associated with formation of [Zn{S_2CN(p-tol)$_2$}$_2$(OLA)]. Two different solvothermal decomposition methods were employed. In heat up (HU) method, a 25 mM pale yellow solution of **2b** in OLA (20 mL) was heated under N_2 in a three-necked round bottom flask. Upon warming to ca. 80 °C the solution turned bright yellow, the colour change being associated with the onset of decomposition [5]. To directly compare with the analogous decomposition of dialkyl-DTC derivatives, heating was continued to 230 °C, at which point the solution was opaque, and was maintained at this temperature for 1 h, which did not alter

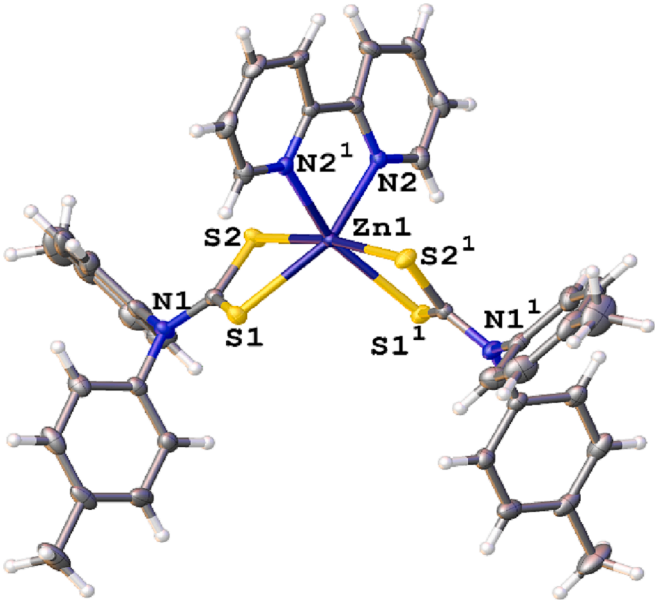

Fig. 4. Molecular structure of [Zn{S_2CN(p-tol)$_2$}$_2$(2,2′-bipy)] (**5**).

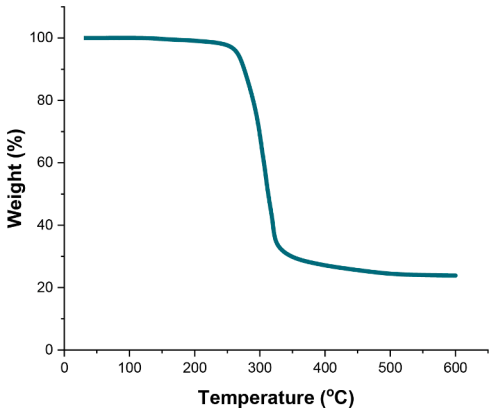

Fig. 5. TGA of [Zn{S_2CN(p-tol)$_2$}$_2$] (**2b**).

the pale-yellow opaque nature of the solution. Slow cooling to room temperature and addition of MeOH led to the precipitation of the generated nanomaterials. These were isolated by centrifugation and washing with MeOH and CH_2Cl_2 to remove organic by-products (see experimental section). This gave a light brown material which was air dried before analysis. We also carried out a hot-injection (HI) decomposition. Here the OLA solution of **2b** was pre-warmed to ca. 70 °C and then injected into a degassed solution of OLA at 230 °C. This resulted in the pale-yellow solution rapidly becoming cloudy. As before, the temperature was maintained at 230 °C for 1 h, and the solids washed as described to afford a light brown powder.

Initial analysis of decomposition materials was by PXRD which for all show the formation of hexagonal ZnS (wurtzite) (Fig. 6). Interestingly, the peak at 28.5° 2θ for the (0 0 2) lattice plane is more intense than in the reference pattern for bulk wurtzite (JCPDS card no. 00–036-1450), which suggests some preferential growth along the c axis. Spectra obtained from both solvothermal processes are broad, indicating that the length scale of the generated nanomaterials is on the order of nm. The selected area diffraction (SAED) pattern (Fig. S1) confirms formation of wurtzite ZnS. TEM images (Figs. 7-8) show that nanorods are produced via both solvothermal methods. Using the HI method, the average length of the rods is 17 ± 3 nm, with minimum and maximum lengths of 11 and 22 nm respectively. The rods are very small with diameters of 2.1 ± 0.5 nm. From the HU method the nanorods are slightly shorter, with an average length 11 ± 3 nm and minimum and maximum lengths 7 and 17 nm respectively but have a larger diameter of 3.5 ± 1.1 nm. This suggests that in both cases, SSP decomposition is rapid, and likely results from amine-exchange, followed by the rapid decomposition of [Zn(S_2CNAr_2)(S_2CNHR)] (R = oleyl). In both cases the rods are shorter than those formed under analogous HU conditions when using [Zn($S_2CN^iBu_2$)$_2$] as the SSP [5] which afforded wires of 34.3 ± 26.2 nm and widths of ca. 2.5–4.0 nm. They are also significantly shorter than those produced upon heating [Zn(S_2CNEt_2)$_2$] in OLA which have lengths of ca. 300 nm and diameters of between 3.0 and 5.5 nm [4].

Dry heating of **2b** affords wurtzite (PXRD) composed of irregular (10–300 μm) sheet-like particles (Fig. 9). They are more crystalline than the solvothermal products, displaying sharper peaks in their PXRD (Fig. 6). The elemental compositions of these sheets were analysed by energy dispersive X-ray (EDX) spectroscopy, mapping showing the proportion of Zn and S to be 65.37 and 34.63 % (by weight) (calculated: Zn 67.07 and S 32.83 %) and 48.08 and 51.92 % by atomic percentage.

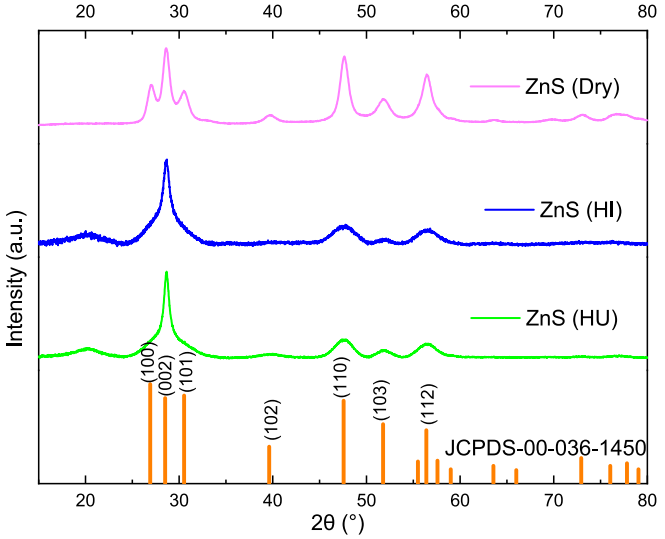

Fig. 6. PXRD for hexagonal ZnS (wurtzite) from [Zn{S_2CN(p-tol)$_2$}$_2$] (**2b**) produced by HU, HI and dry decomposition methods.

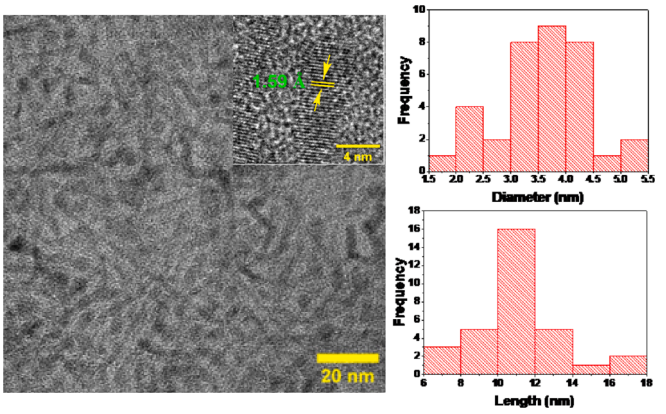

Fig. 7. TEM images of ZnS nanorods produced from **2b** by HU showing average distance between two planes (inset) and histograms of lengths and diameters of the nanorods.

4. Summary and conclusions

We have prepared a number of new Zn(II) diaryl-DTC complexes and shown that their chemistry is similar to that of the well-established dialkyl-DTC derivatives. The latter find quite widespread use as well-known accelerators for the vulcanization of rubber [43,44] and also as SSPs to nanoscale ZnS [1–7] The latter application has been the focus of this work with preliminary studies showing that they are effective SSPs and can be used to prepare nanorods with relatively short lengths and small diameters. This is in contrast with the dialkyl-derivatives which tend to afford either ultrafine nanowires [2–4] or longer nanorods [5]. The smaller size rods generated from [Zn(S_2CNAr_2)$_2$] suggests that the molecular ZnS building blocks are more rapidly formed from this precursor. There are a number of possible explanations for this, two of which are; (i) amine-exchange is faster for aryl than alkyl derivates, and (ii) loss of the secondary DTC ligand is faster from [Zn(S_2CNAr_2){S_2CNH(oleyl)}] than from [Zn(S_2CNR_2){S_2CNH(oleyl)}] (Scheme 1). Thus, following amine-exchange decomposition is very fast as seen for isolated primary-amine derivatives such as [M(S_2CNHR)$_2$] [M = Zn, Cd] [36,45,46]. Probably both amine-exchange and DTC loss are faster for diaryl vs dialkyl DTC complexes. Thus, the electron-withdrawing nature of the aryl ligands should increase the electrophilicity of the backbone carbon, thus facilitating nucleophilic attack by the primary amine [8], while in related Cu(II) chemistry we have shown that loss of a diaryl-DTC ligand from [Cu(S_2CNAr_2)$_2$]$^-$ (when generated electrochemically) is faster than the loss of a dialkyl-DTCs ligand from [Cu(S_2CNR_2)$_2$]$^-$, as shown by the lack of electrochemical reversibility of the former [14]. Whatever the exact reason, our preliminary results suggests that diaryl-DTC complexes [Zn(S_2CNAr_2)$_2$] are a significant addition to the arsenal of SSPs available to prepare ZnS nanomaterials.

CRediT authorship contribution statement

Jagodish C. Sarker: Investigation, Writing – reviewing. **Firoz Alam:** Investigation. **Paul McNaughter:** Investigation. **David Pugh:** Investigation, Reviewing. **Jeremy K. Cockcroft:** Investigation. **David J. Lewis:** Writing – reviewing, Supervision. **Graeme Hogarth:** Conceptualization, Methodology, Writing – reviewing, Supervision.

Declaration of Competing Interest

The authors declare that they have no known competing financial interests or personal relationships that could have appeared to influence the work reported in this paper.

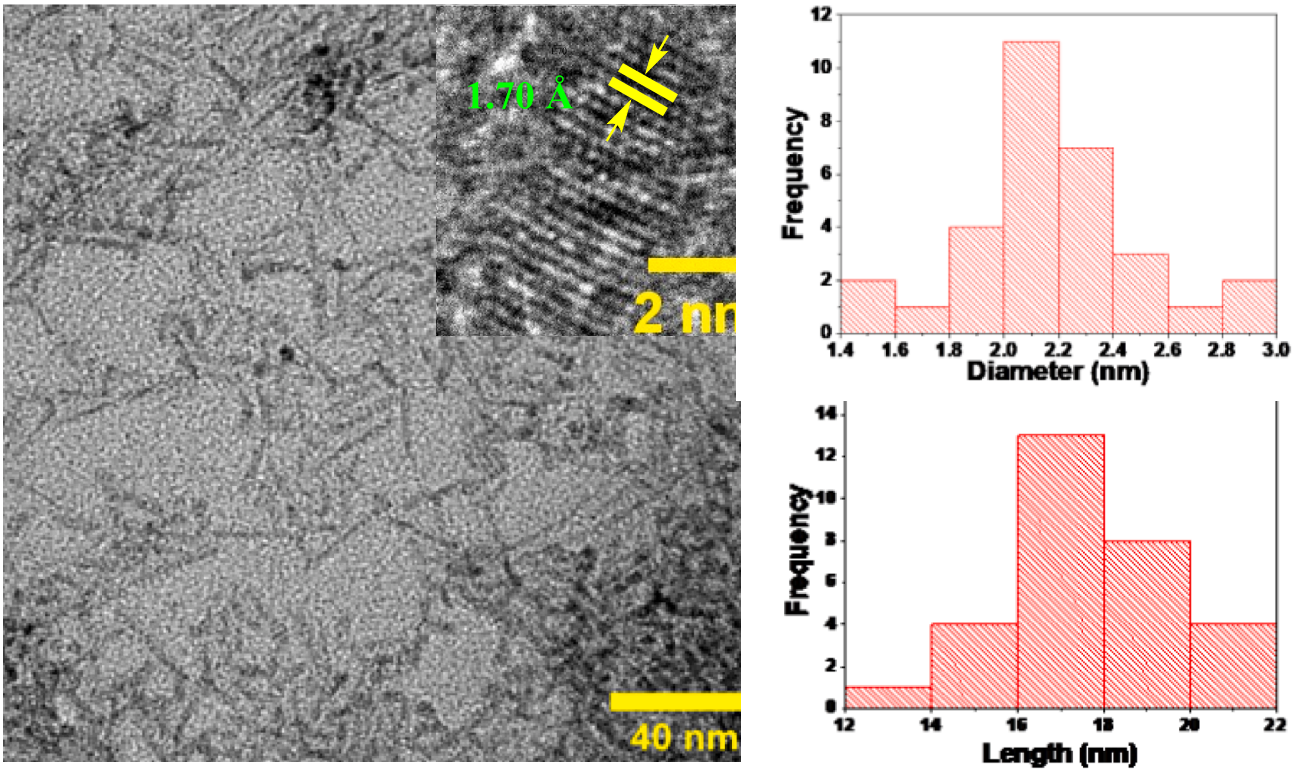

Fig. 8. TEM images of ZnS nanorods produced from **2b** by HI showing average distance between two planes (inset) and histograms of lengths and diameters of the nanorods.

Fig. 9. SEM images of ZnS sheets produced from the dry decomposition of **2b**.

Data availability

Data will be made available on request.

Acknowledgements

We thank the Commonwealth Scholarship commission for a PhD studentship (JCS) and the EPSRC for grants EP/R020590/1 (DJL, FA) and EP/R022518/1 (DJL, P.McN).

Appendix A. Supplementary data

Supplementary data to this article can be found online at https://doi.org/10.1016/j.ica.2023.121663.

References

[1] X. Fang, T. Zhai, U.K. Gautam, L. Li, L. Wu, Y. Bando, D. Golberg, Prog. Mater. Sci. 56 (2011) 175–287.
[2] G. Hogarth, Prog. Inorg. Chem. 53 (2005) 71–561.
[3] J.C. Sarker, G. Hogarth, Chem. Rev. 121 (2021) 6057–6123.
[4] Y. Zhang, H. Xu, Q. Wang, Chem. Commun. 46 (2010) 8941–8943.
[5] H.U. Islam, A. Roffey, N. Hollingsworth, W. Bras, G. Sankar, N.H. De Leeuw, G. Hogarth, Nanoscale Adv. 2 (2020) 798–807.
[6] G. Zhu, S. Zhang, Z. Xu, J. Ma, X. Shen, J. Am. Chem. Soc. 133 (2011) 15605–15612.
[7] Y.C. Zhang, G.Y. Wang, X.Y. Hu, W.W. Chen, Mater. Res. Bull. 41 (2006) 1817–1824.
[8] N. Hollingsworth, A. Roffey, H.-U. Islam, M. Mercy, A. Roldan, W. Bras, M. Wolthers, C.R.A. Catlow, G. Sankar, G. Hogarth, N.H. de Leeuw, Chem. Mater. 26 (2014) 6281–6292.
[9] A. Roffey, N. Hollingsworth, H.-U. Islam, M. Mercy, C.R.A. Catlow, G. Sankar, N. H. de Leeuw, G. Hogarth, Nanoscale 8 (2016) 11067–11075.
[10] A. Roffey, N. Hollingsworth, H.-U. Islam, W. Bras, G. Sankar, N.H. de Leeuw, G. Hogarth, Nanoscale Adv. 1 (2019) 2965–2978.
[11] A. Roffey, N. Hollingsworth, G. Hogarth, Nanoscale Adv. 1 (2019) 3056–3066.
[12] P.B. Mann, I.J. McGregor, S. Bourke, M. Burkitt-Gray, S. Fairclough, M.T. Ma, G. Hogarth, M. Thanou, N. Long, M. Green, Nanoscale Adv. 1 (2019) 522–526.
[13] J.C. Sarker, R. Nash, S. Boonrungsiman, D. Pugh, G. Hogarth, Dalton Trans. 51 (2022) 13061–13070.
[14] J. C. Sarker, X. Xiang, F. Alam, R. Nash, S. Boonrungsiman, J. K. Cockcroft, D. Pugh, D. J. Lewis, G. Hogarth, New J. Chem. (2023) Advance Articlehttps://doi.org/10.1039/D3NJ01918G.
[15] S.J. Coles, P.A. Gale, Chem. Sci. 3 (2012) 683–689.
[16] CrysAlisPRO, Oxford Diffraction /Agilent Technologies UK Ltd, Yarnton, England.
[17] O.V. Dolomanov, L.J. Bourhis, R.J. Gildea, J.A.K. Howard, H. Puschmann, J. Appl. Crystallogr. 42 (2009) 339–341.
[18] L.J. Bourhis, R.J. Gildea, J.A.K. Howard, H. Puschmann, Acta Crystallogr., Sect. A 71 (2015) 59–75.
[19] G.M. Sheldrick, Acta Crystallogr., Sect. C 71 (2015) 3–8.
[20] (a) M. J. Cox, E. R. T. Tiekink, Rev. Inorg. Chem. 17 (1997) 1-23; (b) E. R. T. Tiekink, CrystEngComm 5 (2003) 101-113.
[21] M. Bonamico, G. Mazzone, A. Vaciago, L. Zambonelli, Acta Crystallogr. 19 (1965) 898–909.

[22] H.P. Klug, Acta Crystallogr. 21 (1966) 536–546.
[23] H. Miyame, M. lto, H. Iwasaki, Acta Crystallogr., Sect. B 35 (1979) 1480-1482.
[24] N. Sreehari, B. Varghese, P.T. Manoharan, Inorg. Chem. 29 (1990) 4011–4015.
[25] M. Motevalli, P. O'Brien, J.R. Walsh, I.M. Watson, Polyhedron 15 (1996) 2801–2808.
[26] M.J. Cox, E.R.T. Tiekink, Z. Kristallogr. 214 (1999) 184–190.
[27] S.W. Lai, M.G.B. Drew, P.D. Beer, J. Organomet. Chem. 637–639 (2001) 89–93.
[28] I. Baba, Y. Farina, A.H. Othman, I.A. Razak, H.K. Fun, S.W. Ng, Acta Crystallogr., Sect. E 57 (2001) m51–m52.
[29] I. Baba, Y. Farina, K. Kassim, A. Hamid, A.H. Othman, I.A. Razak, H.K. Fun, S. W. Ng, Acta Crystallogr., Sect. E 57 (2001) m55–m56.
[30] I. Baba, L.H. Lee, Y. Farina, A.H. Othman, A.R. Ibrahim, A. Usman, H.K. Fun, S. W. Ng, Acta Crystallogr., Sect. E 58 (2002) m744–m745.
[31] G. Reck, R. Becker, Acta Crystallogr., Sect. E 59 (2003) m234–m235.
[32] F.A. Almeida Paz, M.C. Neves, T. Trindade, J. Klinowski, Acta Cryst., Sect. E 59 (2003) m1067–m1069.
[33] W.G. Zhang, Y. Zhong, M.Y. Tan, N. Tang, K.B. Yu, Molecules 8 (2003) 411–417.
[34] D.C. Onwudiwe, P.A. Ajibade, Polyhedron 29 (2010) 1431–1436.
[35] N. Srinivasan, S. Thirumaran, S. Ciattini, Spectrochim. Acta Part A: Mol. Biomol. Spectrosc. 102 (2013) 263–268.
[36] D.C. Onwudiwe, C.A. Strydom, Spectrochim. Acta Part A: Mol. Biomol. Spectrosc. 135 (2015) 1080–1089.
[37] D.C. Onwudiwe, Y.B. Nthwane, A.C. Ekennia, E. Hosten, Inorg. Chim. Acta 447 (2016) 134–141.
[38] N.A. Bell, E. Johnson, L.A. March, S.D. Marsden, I.W. Nowell, Y. Walker, Inorg. Chim. Acta 156 (1989) 205–211.
[39] S.M. Zemskova, L.A. Glinskaya, R.F. Klevtsova, V.B. Durasov, S.A. Gromilova, S. V. Larionov, Z. Strukt. Khim. 37 (1996) 1114–1121.
[40] L.A. Glinskaya, R.F. Klevtsova, E.I. Berus, S.M. Zemskova, S.V. Larionov, J. Struct. Chem. 39 (1998) 559–566.
[41] E.R.T. Tiekink, Z. Kristallogr. 216 (2001) 575–576.
[42] S. Khalid, E. Ahmed, M.A. Malik, D.J. Lewis, S. Abu Bakar, Y. Khan, P. O'Brien, New J. Chem. 39 (2015) 1013–1021.
[43] P.J. Nieuwenhuizen, J. Reedijk, M. van Duin, W. McGill, Rubber Chem. Technol. 70 (1997) 368–429.
[44] P.J. Nieuwenhuizen, A.W. Ehlers, J.G. Haasnoot, S.R. Janse, J. Reedijk, E. J. Baerends, J. Am. Chem. Soc. 121 (1999) 163–168.
[45] L.H. van Poppel, T.L. Groy, M.T. Caudle, Inorg. Chem. 43 (2004) 3180–3188.
[46] C.E. Morrison, F. Wang, N.P. Rath, B.M. Wieliczka, R.A. Loomis, W.E. Buhro, Inorg. Chem. 56 (2017) 12920–12929.